Low-Temperature and Photon-Induced Chemistry of Nitrogen on Pt(111)†

R. Zehr, A. Solodukhin, B. C. Haynie, C. French, and I. Harrison*

Department of Chemistry, University of Virginia, Charlottesville, Virginia 22904

Received: September 29, 1999; In Final Form: November 11, 1999

The saturation coverage of N_2 on Pt(111) at surface temperatures below 40 K is $\theta_{sat} = 0.41$ monolayer ± 10%. The N 1s binding energy of 403.8 eV measured by X-ray photoelectron spectroscopy suggests that the preponderance of the N_2 adlayer is physisorbed. Nevertheless, up to 0.07 monolayer of the N_2 was able to very weakly chemisorb on the Pt(111) terraces. This chemisorbed N_2 was assigned as vertically bound to Pt(111) top sites on the basis of its 0.15 eV adsorption energy and 2266 cm^{-1} intramolecular stretching frequency. Thermal programmed desorption, reflection−absorption infrared spectroscopy (RAIRS), and photodesorption data indicate that a 2-D gas phase of chemisorbed N_2 and a condensed N_2 island phase coexist at coverages $\theta \geq 0.07$ monolayer. Within the two-phase regime of coverage, the N_2 thermal desorption kinetics were zeroth order, with a desorption energy of 0.13 eV. The data are broadly consistent with the speculation that the condensed island phase is composed of seven-membered "pinwheels" in which vertically chemisorbed N_2 "pins" are decorated by "wheels" of horizontally oriented physisorbed molecules. Only the weakly chemisorbed N_2 on terrace sites exhibited photodesorption over the 308−193 nm wavelength range. The more strongly chemisorbed N_2 molecules at Pt(111) step defects (identified by a 2234 cm^{-1} band in RAIRS) were photoinactive. The mean translational energy of the photodesorbing N_2 was $\langle E_T \rangle = 0.25 \pm 0.05$ eV ($\langle E_T \rangle / 2k_b \sim 1450$ K), independent of wavelength. The N_2 photodesorption dynamics and action spectra are consistent with a desorption mechanism involving transient attachment of a photoexcited substrate electron into an affinity band of chemisorbed N_2 which lies between 3.5 and 4.0 eV above the Fermi level; presumably the $2\pi^*$ antibonding band. Energy accumulated on the excited state potential prior to quenching back to the ground state drives the photodesorption.

1. Introduction

The interaction of nitrogen with transition metals has been extensively studied because of its importance in the catalytic synthesis of ammonia.[1] Dissociation of N_2 is rate limiting in the industrial production of NH_3 over alkali-promoted Fe catalysts. In order to enhance the rate of reaction of H_2 with N_2 and to optimize the equilibrium yield of NH_3, the industrial synthesis is run at elevated temperatures (∼700 K) and pressures (∼300 bar) which are energetically costly to maintain. Although the development of an alternative low-temperature photosynthesis of NH_3 is an economically attractive goal,[2] studies exploring the possibilities for photochemical activation of N_2 on single-crystal metal surfaces have been lacking. In this paper, we report on the low-temperature thermal properties and ultraviolet photochemistry of N_2 on Pt(111). Very weakly chemisorbed N_2 was found to photodesorb at wavelengths from 308 to 193 nm, whereas physisorbed N_2 was photoinactive. Although N_2 did not photochemically dissociate on the surface, 193 nm photodesorption at a surface temperature of 20 K produced energetic desorbing N_2 with mean translational energies of 0.25 ± 0.05 eV, energies characteristic of a ∼1450 K thermal distribution.

Adsorbate photochemistry on metal surfaces is often driven by photoexcited substrate electrons[3] and there has been sustained theoretical interest in the interaction of N_2 with electrons on transition metal surfaces.[4,5] The electron affinity (EA) of N_2 associated with placing an electron into its $2\pi^*$ lowest unoccupied molecular orbital (LUMO) falls from −2.3 eV in the gas phase to −0.8 eV in the bulk solid phase.[6] High-resolution electron energy loss spectroscopy (HREELS) has determined that a scattering resonance exists for N_2 physisorbed on Ag(111) at an electron beam energy of 1.2 eV.[7] This resonance has been assigned to evolve from the lowest energy electron−molecule scattering resonance of gas phase N_2 (i.e., the $^2\Pi_g$ state of $N_2^-{}_{(g)}$) which is stabilized by roughly an electronvolt by the surface image potential when N_2 is physisorbed at an adsorption height of 3−4 Å.[5] When N_2 is more strongly bound, as might be anticipated to be the case for N_2 on Pt(111), and is certainly the case for N_2 chemisorbed on other transition metals, the affinity level may fall below the vacuum level where it can be accessed through attachment by photoexcited "hot" substrate electrons. An electron-harpooned N_2 is likely to desorb via Antoniewicz bounce dynamics[8] in which the transient anion is attracted toward the surface by the image potential, gains kinetic energy, and after several femtoseconds is neutralized back onto the original adsorption potential where it suffers a collision with the surface and can be "bounced" out into the gas phase if sufficient energy has been accumulated. In this paper, we provide evidence for such photoactivity of adsorbed N_2 and characterize the several chemisorbed and physisorbed N_2 bonding modalities on Pt(111).

2. Experimental Section

Experiments were conducted using an ultrahigh vacuum system whose working pressure was 4×10^{-11} Torr. The UHV system was equipped with rear-view optics for low-energy

* Corresponding author: Phone: (804) 924-3639. Fax: (804) 924-3710. E-mail: harrison@virginia.edu.

† Part of the special issue "Gabor Somorjai Festschrift".

10.1021/jp993490u CCC: $19.00
Published on Web 01/11/2000

electron diffraction (LEED), a double-pass cylindrical mirror analyzer for Auger electron spectroscopy (AES) and X-ray photoelectron spectroscopy (XPS), a 400 W Al/Mg X-ray source, a twice differentially pumped quadrupole mass spectrometer, and an FTIR spectrometer. Two different Pt(111) crystals were used in these experiments, one which could be cooled to 20 K and a second to 27 K. The crystals were cooled through a Cu braid thermal connection to a closed cycle He refrigerator and heated by electron bombardment from a filament located behind the sample. The Pt(111) surfaces were first prepared by cycles of Ar^+ ion sputtering, oxidation at 800 K in an O_2 atmosphere of 10^{-7} Torr, and annealing at 1250 K. After the initial cleanup, the surfaces were most conveniently cleaned by repeated O_2 thermal programmed desorption experiments followed by a temperature flash to 1250 K. The surfaces were judged clean and ready for experimentation when no contaminants were detectable by Auger electron spectroscopy, and more sensitively, by the quality of the final O_2 TPD spectrum. The surface defect densities were calibrated by CO titration as monitored by RAIRS[9] and were found to be ≤ 0.006 monolayer (1 monolayer $= 1.5 \times 10^{15}$ cm^{-2}; the Pt(111) surface atom density).

Angle-resolved TPD spectra were taken with a twice differentially pumped Extrel quadrupole mass spectrometer whose ionizer was located 9.9 cm from the crystal face. The TPD heating ramp was 1.9 K/s. Fourier transform reflection−absorption infrared spectra were measured with a Mattson Galaxy 6020 FTIR at 4 cm^{-1} resolution, averaging 2000 scans over an acquisition time of about 10 min. $^{14}N_2$ (99.998%) from Air Products and $^{15}N_2$ (99.9%) from Isotec were purified with a dry ice−acetone trap before dosing. The latter isotope was used predominantly in thermal programmed desorption experiments in order to avoid background signals due to CO, which has the same mass as $^{14}N_2$.

Dosing was performed by expanding a trapped volume of gas through an effusive doser located 22 mm from the center of the 15 mm diameter Pt(111) crystal. The pressure of the trapped volume was measured with an MKS Baratron Type 122B absolute pressure transducer with a 0−1 Torr range using a PDR-C-2C power supply and readout, which led to a dosing precision of better than 0.3% relative standard deviation as evidenced by comparison of TPD integrals. An absolute exposure scale proportional to the pressure of gas within the trapped volume was established by TPD of CO.[9] The sticking coefficient of CO into its chemisorbed state was coverage independent and presumed to be unity at 20 K. A sharp c(2 × 4) LEED pattern was observed after warming CO multilayers to 300 K which indicates that the saturation coverage of chemisorbed CO is limited to 0.5 monolayer when dosing at 20 K.[9] Given that $\theta_{sat} = 0.5$ monolayer and $S = 1$ for CO, an absolute exposure scale could be fixed by correlating the dosing pressure required to saturate the chemisorbed CO TPD peak with an exposure of 0.5 monolayer.

An excimer laser or harmonics of a Nd:YAG laser were used to irradiate the surface with nanosecond laser pulses of duration from 20 to 6 ns. Time-of-flight (TOF) spectra for the photodesorbing N_2 to reach the quadrupole mass spectrometer were recorded using a multichannel scaler triggered to the laser pulses. Unless otherwise noted the TOF spectra were recorded along the direction of the surface normal and the laser angle of incidence was 50° from the surface normal.

3. Results and Interpretation

3.1. Thermal Programmed Desorption. Figure 1a shows thermal programmed desorption spectra of $^{15}N_2$ after adsorption at $T_s = 27$ K. At the lowest exposures, a broad high-temperature desorption from defect sites was observed over the 65−110 K temperature range. Further dosing led to a relatively sharp desorption peak at $T_P = 52$ K which gradually shifted to 45 K as the exposure was increased to $\epsilon = 0.15$ monolayer. Over this range of exposure, the N_2 thermal desorption kinetics are apparently first order. At $\epsilon = 0.15$ monolayer, the dominant desorption peak at $T_p = 45$ K was best fit by first-order desorption parameters: $\nu_1 = 10^{17}$ s^{-1} and $E_d = 0.15$ eV. At exposures $\epsilon \geq 0.18$ monolayer, the linear segments of the log(TPD rate) vs $1/T$ data of Figure 1b indicate zeroth-order desorption kinetics. The zeroth-order desorption over the exposure range 0.18 monolayer $\geq \epsilon \geq 0.670$ monolayer was characterized by $\nu_0 = 10^{13.6}$ monolayer s^{-1} and $E_d = 0.13$ eV as T_p increased from 45 to 48 K. Bulk N_2 overlayers were difficult to populate at 27 K, but were easily formed on a second Pt(111) crystal by dosing at 20 K. The N_2 multilayers desorbed in TPD at 28 K. Kinetic parameters for the zeroth-order desorption of N_2 multilayers were previously determined by Menzel[10] as $\nu_0 = 10^{12.8}$ monolayer s^{-1} and $E_d = 0.073$ eV.

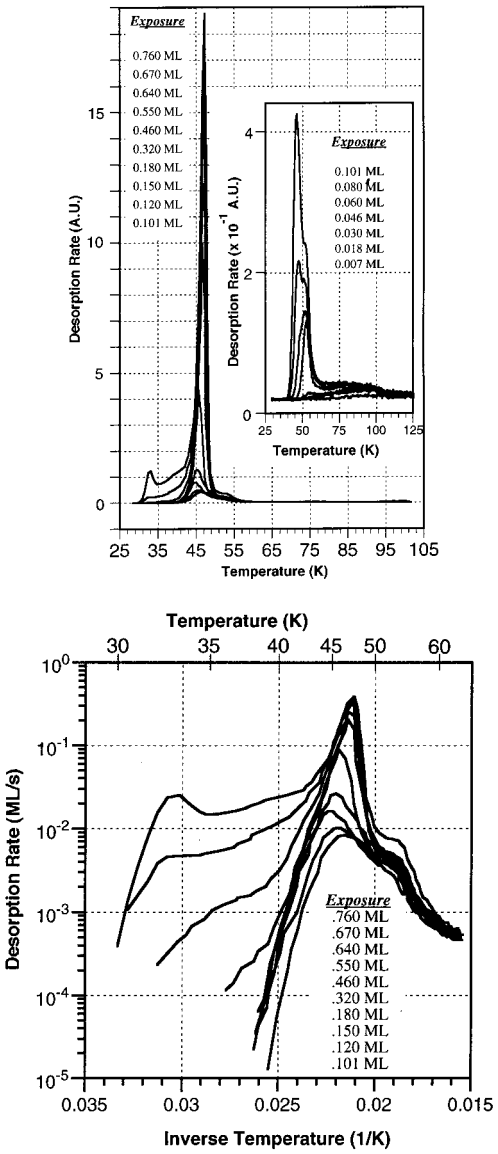

Figure 1. (a, top) Thermal programmed desorption spectra of $^{15}N_2$ ($m/e = 30$) at a series of surface coverages. (b, bottom) Thermal desorption spectra plotted as log(TPD rate) versus $1/T$ to identify the zeroth-order desorption regime.

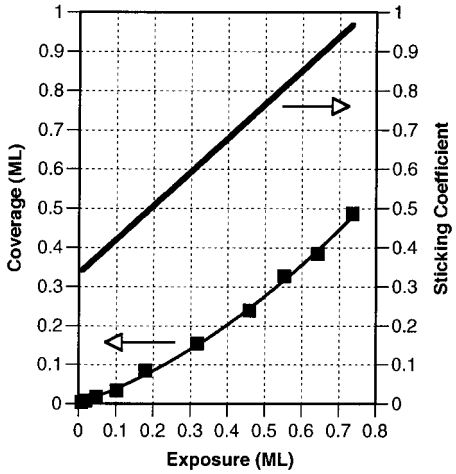

Figure 2. Variation of coverage, θ, and sticking coefficient, S, with exposure, ϵ, when N_2 was dosed on Pt(111) at $T_s = 27$ K. The best fit of $\theta = 0.43\epsilon^2 + 0.33\epsilon$ gave $S = 0.86\epsilon + 0.33$.

The TPD data indicate that the N_2 monolayer, which desorbs in the vicinity of 46 K, behaves much like rare gases on close packed metal surfaces such as Xe on W(110)[11] and Ar on Ru-(001).[12] The nonequilibrium thermodynamics and desorption kinetics of such weakly adsorbed species interacting through van der Waals attractions has been theoretically examined by Kreuzer and Payne.[13] In the rare gas systems, adsorbates form a dilute 2-D gas at low coverage. As the coverage is increased, a condensed 2-D island phase coexists with the dilute 2-D gas phase. Importantly, a constant density 2-D gas is maintained over both the substrate and the condensed islands. In TPD, desorption proceeds out of the 2-D gas and as long as islands are present the overall desorption kinetics are zeroth order. After the island phase is completely depleted, desorption from the remaining 2-D gas becomes first order. The N_2/Pt(111) TPD data are consistent with such a monolayer model in which an island phase coexists with a dilute 2-D gas phase at exposures greater than ~0.18 monolayer.

Figure 2 provides plots of the N_2 coverage, θ, and sticking coefficient, $S = d\theta/d\epsilon$, versus exposure, ϵ. An absolute coverage scale for N_2 was determined by comparison of the integrated N_2 TPD traces to that for 0.5 monolayer of chemisorbed CO, taking into account relative ionization efficiencies and cracking patterns. We estimate our calculated N_2 coverages to be accurate to ±10%. Although our exposures were accurate to better than 1%, henceforth it will generally be more convenient to discuss the experiments in terms of coverage rather than exposure using the experimentally determined relation, $\theta = 0.43\epsilon^2 + 0.33\epsilon$. The TPD spectra show that the N_2 monolayer saturates at $\epsilon \sim 0.67$ monolayer which represents a saturation coverage of $\theta_{sat} \sim 0.41$ monolayer, somewhat lower than the 0.48 monolayer calculated for a close-packed monolayer of the low-temperature α-phase of solid N_2.[14] The low-temperature sticking behavior of N_2 on Pt(111) is quite similar to that observed for N_2 chemisorbing on Ni(111) where the sticking coefficient at 20 K increased smoothly from its initial value of 0.32 ($\theta = 0$) to 0.9 at $\theta_{sat} = 0.52$ monolayer.[15] The initial sticking coefficient of N_2 on Pt(111) of $S_0 = 0.33$ is substantially greater than the $S_0 = 0.23$ value[16] obtained for O_2 on Pt(111) at $T_s = 20$ K, and the $S_0 = 0.12$ value[17] reported for Ar on Ru(001) at $T_s = 6.5$ K. These low initial sticking coefficients are due, in part, to inefficient energy transfer between the adsorbate and substrate caused by poor matching of the adsorbate mass to that of the substrate atoms. Energy transfer is improved at higher coverage when an adsorbing molecule can hit a preadsorbed molecule of the same mass. Translational to rotational energy transfer should increase the sticking for diatomic molecules, which makes it somewhat surprising that the sticking is more efficient for N_2 rather than for O_2 on Pt(111) if both molecules initially adsorb into a physisorbed state (rotational energy level spacings are ~40% larger for N_2). If N_2 on Pt(111) could also chemisorb at low coverage, in a manner similar to N_2 on Ni(111), then the higher N_2, rather than O_2, sticking coefficient on Pt(111) would be more easily understood.

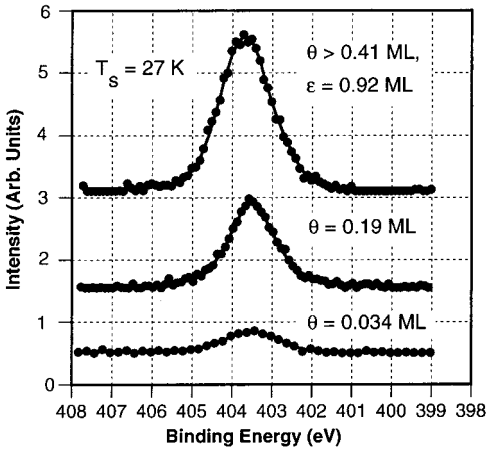

Figure 3. X-ray photoelectron spectra at a series of N_2 coverages.

The strongest binding of N_2 on the Pt(111) surface was at the defect sites. The TPD trace of Figure 1a at $\epsilon = 0.018$ monolayer or $\theta = 0.0062$ monolayer represents desorption from slightly more than the full coverage of defect sites on this Pt-(111) surface. RAIRS observations of N_2 on a (111)-oriented Pt ribbon at 120 K,[18] and on an Ar^+ ion sputtered Pt(111) surface at 90 K,[19] along with the RAIRS data presented below, are consistent with the TPD assignment that nitrogen desorption from defects occurs at considerably higher temperature than from the terrace sites. A density functional electronic structure model for N_2 and CO adsorption on Pt metal surfaces also predicts that the surface bonding should be stronger at the defect sites.[20] Despite enhanced binding at defect sites, our experiments never provided any evidence for thermal or ultraviolet photon induced dissociation of N_2 on Pt(111). At higher excitation energies, it has been reported that 150 eV electron irradiation of N_2 adsorbed on Pt(111) at 100 K induces both desorption and dissociation, presumably for N_2 adsorbed at defect sites.[21]

3.2. X-ray Photoelectron Spectroscopy. Figure 3 shows XPS spectra of N_2 adsorbed on a 27 K Pt(111) surface as a function of coverage. The N 1s electrons show a single XPS peak which shifts slightly toward higher energy with coverage from $E_b(1s) = 403.5$ eV to 403.8 eV. The full width half-maximum of the peak was fwhm = 1.5 eV. We assign this XPS peak to physisorbed N_2 in analogy to N_2 on graphite[22] which has a N 1s binding energy of $E_b(1s) = 403.9$ eV. A N 1s core hole in physisorbed N_2 is only weakly screened by electronic polarization of the surface (i.e., image potential screening) on the femtosecond time scale of the electron photoemission.[23] By contrast, weakly chemisorbed N_2 on transition metals such as Ni(100), W(110), and Ru(001) exhibits a charge transfer screened N 1s "main line" peak at ~400 eV accompanied by a broad "shake up" satellite peak of similar intensity at $E_b \sim 405$ eV.[24] High-resolution XPS spectra of the chemisorbed N_2 show that the main line peak is actually split into two components based on the inequivalence of the two N atoms when the molecule is adsorbed standing up.[25] LEED crystallography has confirmed that N_2 chemisorbs vertically on Ru(001).[26] This is

also presumably the case on other surfaces where N_2 exhibits a doublet N 1s main line. On Fe(111), π-bonded N_2 is chemisorbed parallel to the surface and its XPS spectrum exhibits a singlet N 1s main line at 401.2 eV and a strong satellite peak at 405.9 eV.[27] For even the weakly chemisorbed N_2/metal systems, electronic coupling to the surface is sufficient for substantial charge transfer screening of the N 1s core hole to be observed in XPS. The N 1s main line is assigned to a fully screened final state in which one electron has been transferred from the substrate into the $2\pi^*$ screening orbital of the core-ionized N_2.[23] The strong shake up satellite peak appearing at 4−6 eV higher binding energy accompanies transitions of the $2\pi^*$ screening electron into Rydberg-like 3s, 3p, and 4p derived final states.[23] The important point to be made here is that chemisorbed N_2 on other metals exhibits an easily recognizable XPS signature and no trace of this signature could be detected for N_2 on Pt(111).

A final argument for the assignment of N_2 as physisorbed on Pt(111) comes from the similarity of its XPS spectrum with that for physisorbed N_2 on Ni(111).[15] On a Ni(111) surface at 20 K, half the coverage of N_2 in the monolayer directly contacting the surface is chemisorbed while the other half is physisorbed. The N_2/Ni(111) XPS spectrum showed the characteristic N 1s main line and satellite peaks of chemisorbed N_2 along with a single additional peak at $E_b(1s) \sim 403.5$ eV with fwhm = 1.5 eV derived from physisorbed N_2. Both the binding energy and peak shape of the N 1s XPS peak for physisorbed N_2 on Ni(111) match those for N_2 on Pt(111).

3.3. Reflection−Absorption Infrared Spectroscopy. Although gas phase N_2 does not absorb infrared, RAIRS studies of chemisorbed N_2 on Ni(110),[28] Ni(111),[29] Ru(001),[30] Ir(100),[31] and defects of Pt(111) surfaces[18,19] show strong absorption bands associated with the N_2 intramolecular stretching vibration. In RAIRS on metal surfaces, only adsorbate modes associated with dipole derivatives with a component projecting onto the infrared electric field oriented along the surface normal may exhibit absorption bands. Furthermore, to observe N_2 by RAIRS the bonding at the surface must be sufficiently strong to break the molecular inversion symmetry and induce a nonzero dipole derivative associated with the N_2 stretching mode. To date, RAIRS spectra of N_2 on transition metals have only been observed in cases where the molecules were at least weakly chemisorbed and oriented vertically on the surface. Physisorbed N_2 should not display RAIRS bands.

Figure 4a shows an infrared spectrum of $\theta = 0.27$ monolayer N_2 dosed on the surface at 20 K and a second spectrum taken after the surface was annealed for several seconds at 67 K. After the terrace N_2 was desorbed by annealing to 67 K, only a single absorption band at 2234 cm^{-1} remained. A similar band at 2222 cm^{-1} was previously assigned to N_2 adsorbed on monovacancy defects created by Ar^+ ion sputtering of a Pt(111) surface at 90 K.[9] When the Ar^+-sputtered surface was annealed (to $\leq$700 K) and the monovacancies could aggregate into vacancy islands (presumably with monatomic step edges[32]), the RAIRS absorption band measured at 90 K shifted from 2222 to 2242 cm^{-1}. These experiments establish a spectral range for RAIRS activity of N_2 adsorbed on a variety of possible surface defect structures. We assign the broad 2234 cm^{-1} band of Figure 4a to N_2 adsorption at the only known defects of our well-annealed surface,[7] the step edge sites. These step edge sites were identified after adsorption of CO by a distinctive CO RAIRS band at 2068 cm^{-1}.[33] When the step sites were blocked by preadsorbing a small quantity of CO (ca. 0.006 monolayer) and annealing to 250 K, postdosing N_2 at 27 K produced a RAIRS absorption band at 2266 cm^{-1} but negligible absorption at 2234 cm^{-1}.

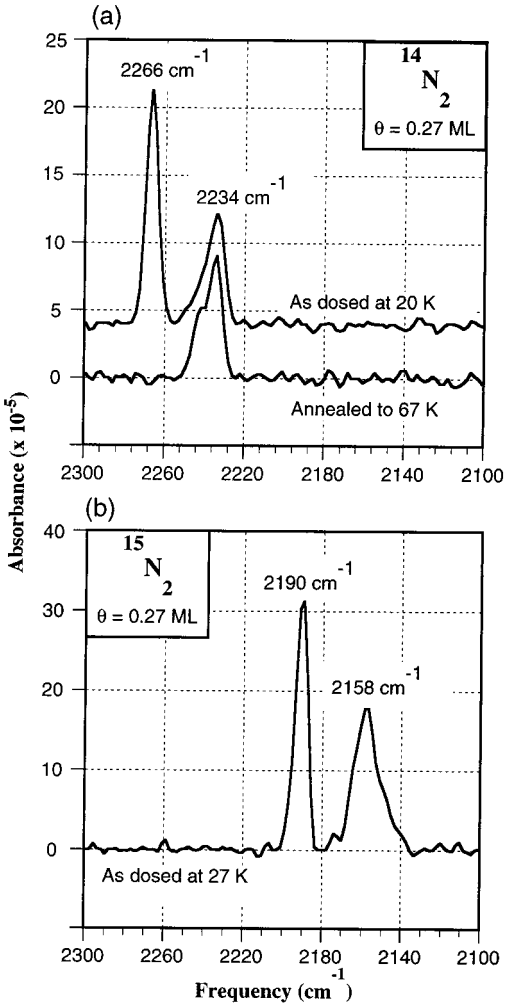

Figure 4. RAIRS spectra for 0.27 monolayer coverages of (a) $^{14}N_2$ and (b)$^{15}N_2$ on two different Pt(111) surfaces.

The stronger absorption band at 2266 cm^{-1} in Figure 4a disappeared when the terrace N_2 was desorbed by annealing the surface to 67 K. In consequence, this band is tentatively assigned to N_2 molecules adsorbed at terrace sites. A considerably higher intramolecular stretching frequency of 2331 cm^{-1} is measured by Raman spectroscopy for gas phase N_2.[34] The substantial downward frequency shifts of $\Delta\nu = 65$ cm^{-1} for terrace N_2 and $\Delta\nu = 97$ cm^{-1} for defect bound N_2 suggest that the electronic structure of the RAIRS active adsorbates is considerably altered from the gas phase. The frequency shift was larger for the more strongly bound N_2 at the defect sites which desorbed at higher temperature. The assignment of the vast majority of the N_2 monolayer as physisorbed by XPS requires that the RAIRS bands be derived from a minority of chemisorbed N_2. On symmetry grounds, it is likely that both the RAIRS-active terrace and defect bound N_2 bind with internuclear axis perpendicular to the surface plane (and thereby couple well to the surface infrared). Figure 4b shows the isotopic shift of the vibrational bands when $^{15}N_2$ is substituted for $^{14}N_2$. The heavier isotope exhibits bands at 2189 and 2158 cm^{-1} which are consistent with chemisorbed N_2 oscillating harmonically at the terrace and defect sites. No additional RAIRS bands were observed when physisorbed N_2 overlayers were adsorbed at 20 K.

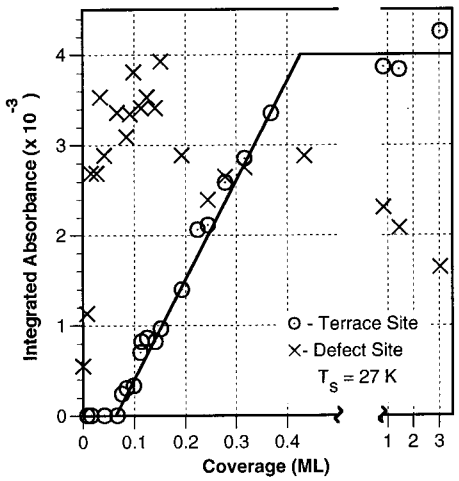

Figure 5. Integrated intensity of the N_2 RAIRS bands for adsorption on the terrace and defect sites as a function increasing $^{15}N_2$ coverage at $T_s = 27$ K.

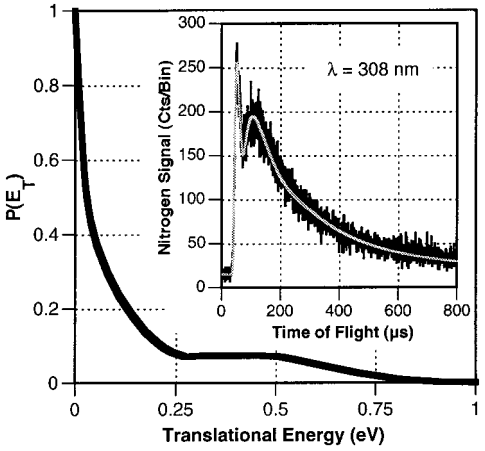

Figure 6. Translational energy distribution, $P(E_T)$, for nitrogen photodesorbing along the surface normal at 308 nm for $\theta = 0.27$ monolayer of $^{14}N_2$. Inset shows the associated time-of-flight spectrum ($m/e = 28$) and the fit generated from the $P(E_T)$.

The evolution of the N_2 RAIRS bands with increasing coverage at a surface temperature of 27 K are given in Figure 5. The defect band absorbance increases with coverage until about 0.04 monolayer, saturates, and then slowly diminishes as the coverage is increased past 0.14 monolayer. Given that the defect band could be completely quenched by adsorbing only 0.006 monolayer CO at the defects, there is apparently a dynamic equilibrium between N_2 adsorbed at defects and on the terraces at higher coverages. The ultimate rollover in the defect band intensity with coverage may derive from dipole coupling to the higher frequency terrace N_2 band,[35] a change in the N_2 bonding at defects, or changes in the surface electrodynamics of the system brought about by coadsorbed N_2 at terrace and overlayer sites.[36]

Most interesting about Figure 5 is that the terrace band absorbance grows in linearly with coverage beginning at 0.07 monolayer (>10 times the surface defect level). This behavior is consistent with a RAIRS inactive phase of N_2 being joined by a second RAIRS active phase in two-phase coexistence for coverages $\theta \geq 0.07$ monolayer. If only a single phase of terrace N_2 could be supported on the surface at a given time, there would have been a step change in the integrated absorbance at $\theta = 0.07$ monolayer as the new phase appeared. The RAIRS data are consistent with the TPD results which indicate that terrace N_2 exists as a dilute 2-D gas at low coverages but that an island phase begins to coexist for coverages $\theta \geq 0.07$ monolayer. In consequence, the 2266 cm^{-1} band is assigned to RAIRS active molecules within the terrace islands. If the RAIRS cross section for these molecules is comparable to those on defects, the total coverage of RAIRS active molecules in the condensed islands is only ~0.006 monolayer. This would be in accordance with the detection of only physisorbed N_2 in XPS and prompts a more specific assignment of the terrace RAIRS band to a minority species within the condensed islands. It appears likely that the RAIRS active molecules are found within the interior, rather than the perimeter, of the islands because both the peak position, 2266 ± 0.7 cm^{-1}, and fwhm, 7.9 ± 0.6 cm^{-1}, of the terrace RAIRS band were independent of coverage within the monolayer, indicative of an unchanging local environment surrounding the RAIRS active molecules. It may be that imperfections within the islands, such as domain walls, force some molecules into relatively unfavorable, upright geometries where they become electronically chemisorbed and RAIRS active. Alternatively, it may be that the islands consist of N_2 "pinwheels", similar to those found on Cu(110),[37] in which each vertically oriented "pin" molecule is surrounded by six horizontal molecules which make up the wheel. If the vertical pin molecules were weakly chemisorbed on the Pt(111) surface, they would form a relatively homogeneous set of RAIRS active molecules which could explain the coverage independence of the RAIRS band characteristics. Figure 5 suggests that the terrace absorbance provides a measure of the island phase coverage within the monolayer. If the condensed islands consist of seven-membered N_2 pinwheels, then as much as 0.06 monolayer, or one-seventh of the 0.41 monolayer saturation coverage of the N_2 monolayer, could be vertically chemisorbed. In this case, Figure 5 requires the RAIRS absorption cross section for the N_2 weakly chemisorbed within the terrace islands to be an order of magnitude smaller than for N_2 chemisorbed at the stronger binding defect sites. This is not unreasonable since any RAIRS activity depends on breaking the local inversion symmetry of N_2 through bonding to the surface.

3.4. Low-Energy Electron Diffraction. There was no evidence by low-energy electron diffraction (LEED) that N_2 formed an ordered overlayer on Pt(111) when the electron beam energy was limited to $E_{el} \leq 50$ eV. However, when the surface was exposed to the 1 μA electron beam at beam energies above about 100 eV a 2 × 2 pattern developed over irradiated regions of the surface. It is likely that the LEED pattern derives from N atoms dissociated by the energetic electron beam. N atom ordering on Pt(111) to give 2 × 2 LEED patterns has previously been observed when N atoms were produced by thermal reaction between coadsorbed NH_3 and O atoms.[38]

3.5. N_2 Photodesorption. Molecular nitrogen on Pt(111) was found to photodesorb under ultraviolet laser irradiation at 193, 266, and 308 nm, but not at 355 or 532 nm. Figure 6 gives the N_2 time-of-flight (TOF) spectrum and associated translational energy distribution, $P(E_T)$, for a 0.27 monolayer coverage of $^{14}N_2$ irradiated at 308 nm at a surface temperature of 20 K. The mean translational energy of N_2 desorbing along the surface normal is $\langle E_T \rangle = 0.20$ eV ($\langle E_T \rangle / 2k_b \sim 1200$ K) and the maximum desorption energy is roughly $E_T^{max} = 0.8$ eV. The bimodal distribution can be split at $E_T = 0.25$ eV (75 μs in TOF) into fast and slow components with mean translational energies of 0.48 and 0.08 eV, respectively. The fast N_2 is thought to have photodesorbed directly from the surface. The slow N_2 may have suffered energy degrading collisions during exit from the adlayer. Interadsorbate quenching may also reduce the kinetic energy of the desorbing N_2 by reducing the time spent on the accelerating excited state potential. The translational energy

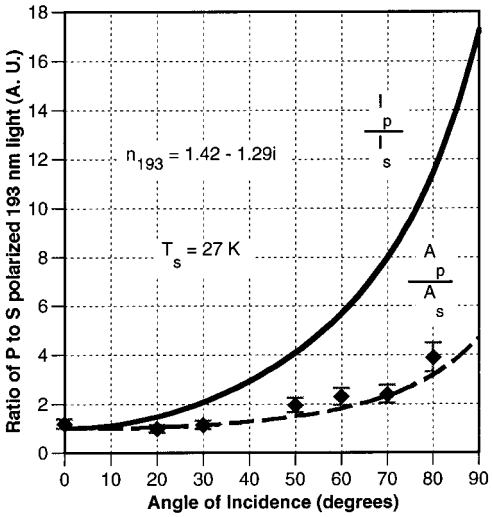

Figure 7. Ratio of the 193 nm photodesorption yields for p- versus s-polarized light as a function of angle of incidence for irradiation by 8×10^{18} photons/cm^2.

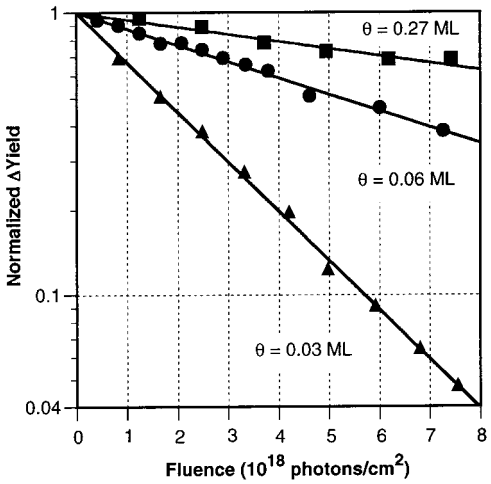

Figure 8. Decrease of the incremental photodesorption yield in $^{15}N_2$ TOF spectra as a function of 193 nm fluence for three different initial coverages of N_2.

distributions were coverage dependent and the relative yield of the slow N_2 component increased with coverage. When the laser excitation wavelength was shifted from 308 nm to shorter wavelengths, the photodesorption cross section increased, but the N_2 translational energy distribution remained essentially constant (e.g., $\langle E_T \rangle = 0.21$ eV at 193 nm and $\theta = 0.27$ monolayer).

Polarization experiments were conducted in which the photodesorption yields were monitored by TOF spectroscopy as a function of the laser angle of incidence and polarization. Figure 7 shows the ratio of the photodesorption yields for p- versus s-polarized light, Y_p/Y_s, as a function of laser incidence angle for 193 nm irradiation by 8×10^{18} photons/cm^2. The ratio of the photodesorption yields tracks the ratio of the calculated polarized light absorptions for the Pt substrate, A_p/A_s, rather than the ratio of the surface electric field intensities. The photodesorption behavior is consistent with a substrate mediated photoprocess involving transient attachment of photoexcited substrate carriers (electrons or holes) to an affinity level of the adsorbed N_2, or an electronic excitation of N_2/metal complexes with a transition moment in the surface plane.[39] The invariance of the N_2 translational energy distribution and the increase in the photodesorption cross section as the photon energy was increased from 4.0 eV (308 nm) to 6.4 eV (193 nm) are diagnostic of the former, "hot" carrier, mechanism. If photons directly excited an electronic transition of N_2/metal complexes then the translational energy distribution of the photodesorbing N_2 should have varied as the photon energy was tuned and different Franck−Condon regions of the upper state potential were accessed. Furthermore, the Franck−Condon overlap between the ground and excited states in a direct transition localizes the photoexcitation spectrum such that it should eventually roll off at high photon energies, not slowly increase. By contrast, photoexcited electrons are produced in a continuum up to the Fermi energy plus the photon energy ($E_F + h\nu$), when the laser irradiates the surface such that the nuclear dynamics following electron attachment to an adsorbate should be independent of photon energy as long as $E_F + h\nu$ remains above the top of the adsorbate affinity band.[3] Under the last condition, the cross section is likely to increase with photon energy as more photoexcited substrate electrons are able to cascade downward into the energy range of the affinity band through inelastic electron−electron scattering.[40] In summary, the experimental data support a substrate mediated photoexcitation mechanism involving hot carriers transiently attaching into an adsorbate affinity band. On the basis that the electronic coupling between the surface and a weakly adsorbed molecule should be greatest between the more diffuse electronically excited orbitals we are generally inclined to discount the participation of hot holes in photodesorption and favor mechanisms involving hot substrate electrons. In consequence, we will explicitly discuss photodesorption mechanisms involving hot electrons below with the implicit understanding that hot holes could act quite similarly.

The net cross sections for N_2/Pt(111) photochemistry were measured by TOF spectroscopy. Figure 8 shows the diminishment of the incremental photodesorption yield measured by TOF spectroscopy as a function of 193 nm fluence for several different initial coverages of N_2. Here, the incremental photodesorption yields accumulated over successive 500 laser shot experiments are plotted, and fitted to first-order exponential decay curves to extract the net photochemical cross sections, σ. The net cross section is the sum of all cross sections associated with processes that diminish the number of photoactive molecules on the surface. Photodesorption may be only one of these processes. We assume that the photoactive coverage obeys the defining equation

$$d\theta_A/dt = -\sigma F \theta_A \tag{1}$$

so that

$$\theta_A = \theta_{A0} e^{-\sigma F t} = \theta_{A0} e^{-\sigma F} \tag{2}$$

where F is the photon flux, F is the fluence, and t is time. Then, the incremental photodesorption yield in the TOF spectra, ΔYield, measured for constant increments of fluence, F_Δ, should obey

$$\Delta\text{Yield} \propto \theta_{A0} e^{-\sigma F}(1 - e^{-\sigma F_\Delta}) \tag{3}$$

which adequately describes the data of Figure 8. The linearity and varied slopes of the Figure 8 data plots indicate that the net photochemical cross section depends on the *initial* coverage of N_2, and not on the evolving N_2 coverage which diminishes during an irradiation experiment. Electron-stimulated desorption (ESD) of CO from W(110) and Cu_x/W(110) at 90 K showed similar behavior in which the ESD cross section depended on

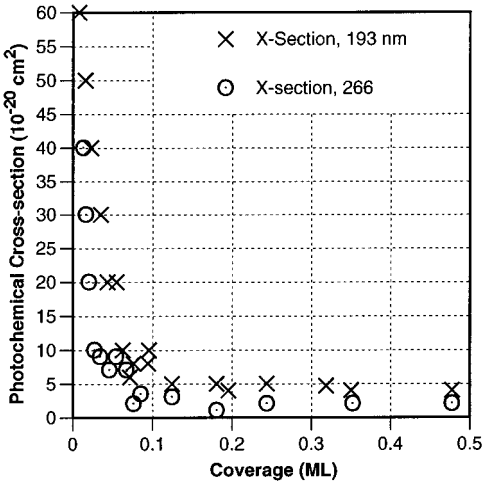

Figure 9. 193 and 266 nm photochemical cross sections as a function of coverage.

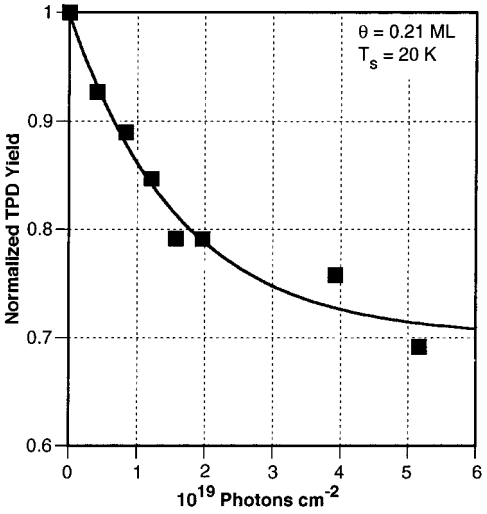

Figure 10. TPD measured decrease of the $^{15}N_2$ coverage as a function of 193 nm fluence beginning with $\theta = 0.21$ monolayer. The best fit line is normalized TPD yield $= (0.147 + 0.063e^{-\sigma F})/0.21$, where $\sigma = 6.2 \times 10^{-20}$ cm^{-2} and F is the fluence.

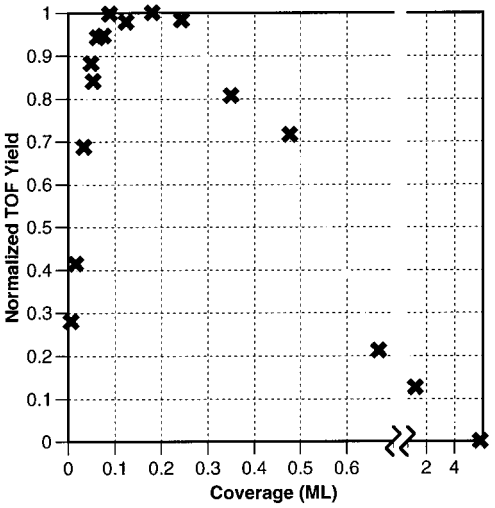

Figure 11. Coverage dependence of the 193 nm photodesorption yield of $^{15}N_2$ from TOF spectra for an accumulated fluence of 10^{19} photons/cm^2 at $T_s = 20$ K.

only the initial CO coverage.[41] If individual molecules undergoing nonthermal desorption by electronic transitions (DIET) do not alter the local adsorbate configuration or bonding of nearby molecules, and if thermal equilibrium is not maintained at low temperature, then the DIET cross sections are expected to depend on only the initial adsorbate coverage.

Figure 9 plots the N_2 photochemical cross sections derived by TOF spectroscopy as a function of coverage for irradiation at 193 and 266 nm. The cross sections at both wavelengths varied similarly with coverage, but the 266 nm cross section was typically ~50% smaller than the 193 nm cross section. The cross sections peaked at zero coverage and diminished rapidly with increasing coverage until stabilizing at steady values for $\theta \geq 0.07$ monolayer within the submonolayer regime of coverage. The RAIRS and TPD results indicate that up until $\theta = 0.07$ monolayer the N_2 exists as a dilute 2-D gas, and further coverage leads to two-phase coexistence with an additional condensed island phase. In consequence, Figure 9 suggests that the dilute 2-D gas of N_2 is the photoactive phase. When only the 2-D gas is present at low coverages, photodesorption is still observed. The reduction of the photochemical cross sections with coverage can be rationalized on the basis of increased interadsorbate quenching as the mean separation between N_2 molecules is reduced. The TPD data of Figure 1 show that the first-order desorption at low coverages shifts toward lower temperature with coverage and this in turn indicates that entropy or repulsive interactions between the N_2 (at least at long range) tend to keep the molecules apart in the dilute 2-D gas. Eventually, a critical density is reached and attractive interactions facilitate local N_2 condensation into islands. Nitrogen molecules in the condensed island phase do not appear to be photoactive because there is little to no modulation of the photochemical cross sections or TOF spectra with coverage as this phase continues to grows in beyond $\theta = 0.07$ monolayer.

The N_2 photodesorption cross section was measured independently by thermal programmed desorption following irradiation of the N_2/Pt(111) surface. Figure 10 shows the decrease of the N_2 coverage with irradiated fluence at 193 nm for an initial coverage of $\theta = 0.21$ monolayer. The data were best fit to a two-component model of the monolayer

$$\theta = \theta_I + \theta_{A0}e^{-\sigma F} \qquad (4)$$

in which some of the coverage is photoactive, θ_A, and the remainder is photoinactive, θ_I. In this instance, the fit gave $\theta_{A0} = 0.063$ monolayer with $\sigma = 6.2 \times 10^{-20}$ cm^{-2}. Significantly, the photodesorption cross sections measured by TPD in this manner match the net photochemical cross sections measured by TOF spectroscopy in Figure 9. In consequence, the two-phase model of the monolayer with $\theta_A \leq 0.07$ monolayer seems robust and photodesorption appears to be the only photochemical process that removes photoactive molecules from the surface.

Figure 11 shows the coverage dependence of the 193 nm photodesorption yield of N_2 measured by TOF spectroscopy after a fluence of 10^{19} photons/cm^2 at $T_s = 20$ K. The yield increased monotonically until a coverage of $\theta \sim 0.07$ monolayer was reached. The N_2 yield remained constant with increasing coverage as the island phase grew in but began to fall as the monolayer saturated. As overlayers grew in the photodesorption yield gradually diminished to negligible levels in the limit of bulk N_2 solid. This behavior is consistent with the dilute 2-D gas being the photoactive phase. As the 2-D gas density increases with coverage the desorption yield increases until it saturates at the critical density which coexists with the condensed island phase. Afterwards, if the dilute 2-D gas exists over both the substrate and the islands, the photodesorption yield should remain constant as the overall coverage is increased. The

decrease of the photodesorption yield as overlayers are formed may be due to elimination of the dilute 2-D gas phase, collisional suppression of desorption by a photoinactive overlayer, a falloff in the flux of photoexcited substrate electrons that can reach the outermost N_2 molecules, or an upward energy shift of the adsorbate affinity level which renders it inaccessible to the photoexcited substrate electrons. The initial falloff in the photodesorption yield at close to saturation coverage suggests that some overlayer molecules may be present at $T_s = 20$ K before the monolayer is completed. TOF spectroscopy of the photodesorbing N_2 indicates that the photoactive species underwent first-order decay (e.g., Figure 8) with the cross sections given in Figure 9 even for $\theta \geq 0.07$ monolayer. In consequence, it appears that equilibrium was not maintained between the dilute gas phase and the condensed island phase during irradiation at $T_s = 20$ K. If thermal equilibrium had been maintained, then the lattice gas coverage and density would have remained invariant as long as islands were present on the surface. In equilibrium, the photodesorption yield kinetics would have been zeroth order and no decay would have been seen until the island phase was completely depleted (i.e., similar to the TPD kinetics). Our observations of incomplete equilibrium between the dilute 2-D gas and island phases for N_2/Pt(111) during photodesorption have analogues in the TPD observations of Menzel and co-workers for rare gas/Ru(001) systems[12] which exhibit similar two-phase behavior. Menzel found that very different desorption rates (by a factor of as much as 8) could be observed if a certain coverage was prepared by direct absorption or by starting with a large coverage and desorbing down to the smaller coverage of interest. Such hysteresis in their thermal desorption results indicates that complete phase equilibrium was not achieved during TPD despite passage through the desorption temperature. In our photodesorption experiments, attempts to modulate the apparent N_2 disequilibrium by changing the laser repetition rate from 2 to 20 Hz and by varying the surface temperature from 20 to 40 K did not discernibly alter the N_2 photochemical cross sections, yields, or dynamics. We suspect that the ~0.15 eV heat of adsorption of the N_2 molecules suffices to anneal the adlayer during the adsorption process but that thermal energies at $T_s \leq 40$ K (i.e., $kT \leq 0.003$ eV) are insufficient to maintain equilibrium during laser irradiation.

Given that the maximum coverage of the photoactive 2-D gas phase of adsorbed N_2 was relatively small, $\theta_A \leq 0.07$ monolayer, it was important to determine whether N_2 adsorbed at defects or other minority sites were photoactive contributors to the overall photodesorption. As discussed earlier in sections 2 and 3.3, the defects of the two Pt(111) crystals used in these studies amounted to less than 0.006 monolayer of step edge sites as measured by CO titration using RAIRS. Two experiments were performed to test for photoactivity of N_2 at step sites. In the first, a N_2-dosed surface was irradiated at 193 nm at a surface temperature of 80 K where RAIRS showed full occupancy of N_2 at step sites (band at 2234 cm^{-1} as in Figure 4a) but no terrace N_2 could be seen in RAIRS nor is it expected based on TPD (Figure 1). No photochemical activity of the step site N_2 could be measured by our spectroscopic techniques. In the second experiment, the surface step sites were blocked and decorated by CO (as confirmed by RAIRS) and then postdosed with N_2 at 20 K before irradiation at 193 nm. The N_2 photodesorption dynamics were the same as those for neat N_2 deposited at 20 K. We conclude that the N_2 chemisorbed at the step defects is photoinactive and does not contribute to our photodesorption signals.

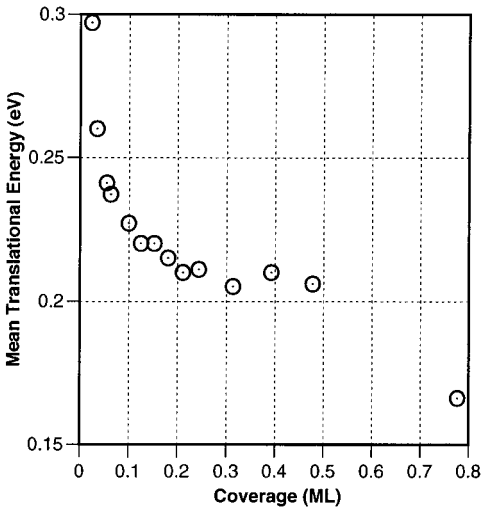

Figure 12. Mean translational energy, $\langle E_T \rangle$, of photodesorbing $^{15}N_2$ at 193 nm as a function of coverage. The 193 nm fluence was 8×10^{18} photons/cm^2.

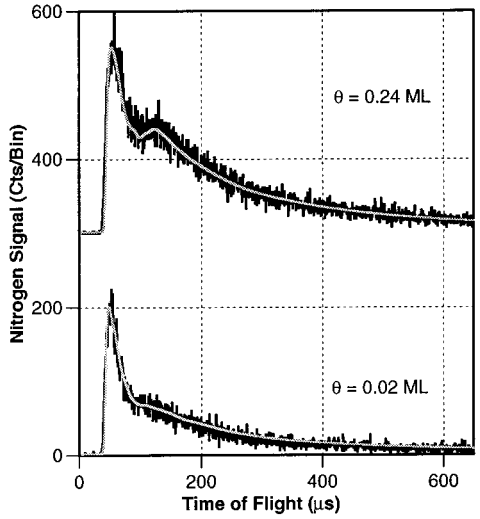

Figure 13. Time-of-flight spectra for $^{15}N_2$ irradiated with 8×10^{18} 193 nm photons/cm^2 at two different initial coverages of N_2. The spectra are offset by 300 counts/bin.

The N_2 photodesorption dynamics varied slowly with coverage. Figure 12 plots the mean translational energy, $\langle E_T \rangle$, of N_2 photodesorbing at 193 nm versus coverage. Bimodal TOF spectra similar to Figure 6 were observed at all coverages but the fraction of molecules appearing in the slow peak, at times $t \geq 75$ μs, increased with coverage until $\theta = 0.07$ monolayer was exceeded. Accordingly, the mean $\langle E_T \rangle$ fell from 0.30 eV at $\theta = 0.02$ monolayer to 0.21 ± 0.02 eV for coverages from 0.07 to 0.48 monolayer. Figure 13 shows the evolution of the 193 nm TOF spectra as the density of the 2-D lattice gas phase was increased.

At fixed coverage, the translational energy distributions of N_2 photodesorbing at 193 nm (Figure 12), 266 nm, and 308 nm (Figure 6) were experimentally indistinguishable. As discussed above in the context that photodesorption occurs via transient attachment of a photoexcited substrate electron into an affinity band of adsorbed N_2, strict invariance of the N_2 translational energy distributions with changing wavelength requires that the affinity band be consistently located below $E_F + h\nu$. In consequence, an energetic upper bound for the affinity band is 4.0 eV above the Fermi level because the N_2 translational energy distribution remained constant for excitation wavelengths

as long as 308 nm ($h\nu = 4.0$ eV). A lower energy bound for the affinity band is provided by the fact that we observed no photoactivity of adsorbed N_2 when the surface was irradiated at 355 nm ($h\nu = 3.5$ eV) and 532 nm ($h\nu = 2.3$ eV). In summary, these data indicate that the affinity band lies between 3.5 and 4.0 eV above the Fermi level.

4. Discussion

4.1. Thermal Chemistry. Let us briefly summarize our major findings based on the data presented above before going on to discuss the electronic structure rationale for N_2 being predominantly physisorbed rather than chemisorbed on Pt(111). The XPS spectra indicate that the majority of the N_2 monolayer adsorbed on Pt(111) at $T_s \leq 27$ K is physisorbed. TPD shows that the weakly adsorbed N_2 exists as a 2-D gas at coverages less than 0.07 monolayer and that a condensed 2-D island phase coexists at higher coverage. Simple analyses of the zeroth- and first-order TPD kinetics indicate that submonolayer N_2 binding energies are in the 0.13−0.15 eV range, somewhat higher than the 0.08 eV heat of sublimation for bulk solid N_2 and thick multilayer deposits. Distinct RAIRS absorption bands were observed for N_2 chemisorbed at defects and for the minority of N_2 chemisorbed within the interior of condensed islands of physisorbed N_2, likely within pinwheel structures or at island domain walls.

A. Bonding. Surface electronic structure calculations based on density functional theory (DFT) have recently led to the conclusion that the bonding of N_2 and isoelectronic CO to transition metal surfaces are qualitatively very similar,[42] even though the quantitatively disparate adsorption properties of these molecules might suggest otherwise.[30] Following Blyholder,[43] the bonding of the vertically chemisorbed molecules can be viewed as the result of favorable electron donation from the filled molecular 5σ orbital into the metal and favorable back-donation from the metal into the empty molecular $2\pi^*$ antibonding orbitals overcoming the Pauli repulsions introduced as the molecular orbitals overlap with those of the metal.[44] Nørskov has shown that by first coupling the metal sp states to the molecular states and subsequently coupling the hybrid states to the metal d states, quantitative DFT calculations of the molecular bonding may be successfully decomposed into contributions relating to the various components of the Blyholder bonding model.[45] The strongest contribution to the surface bonding comes from the $2\pi^*$ back-donation while the most destabilizing interaction is 5σ repulsion. The weaker bonding of N_2 as compared to CO stems primarily from poorer coupling of $2\pi^*$ states to the metal d states. From the gas phase molecular wave functions, it is clear that there is more weighting of the $2\pi^*$ orbital on the atom closest to the surface for CO than for N_2. It is this weighting which scales the overlap with the metal d orbitals and hence the state coupling. The DFT calculations for N_2 and CO on Ru(001) are able to nearly quantitatively reproduce the experimental values for the molecular adsorption energies, bond lengths, and vibrational frequencies.[42] The calculations also provide an interesting explanation for the greater reduction of the intramolecular stretching frequency upon adsorption for N_2 as compared to CO, despite weaker back-donation from the metal d states into the $2\pi^*$ orbital for N_2. By itself, back-donation into the antibonding $2\pi^*$ orbital should reduce the bond strength and hence the vibrational stretching frequency. However, in the case of CO, donation of electrons into the metal from the 5σ orbital generates an opposing upward frequency shift. This is because the lone pair in the asymmetric 5σ orbital of gas phase CO polarizes the 1π orbital which decreases the bonding and vibrational frequency. When the 5σ orbital is depleted upon adsorption, the 1π state becomes less polarized and the vibrational frequency is pushed upward. The opposing effects of the 5σ donation and $2\pi^*$ back-donation on the strength of the intramolecular CO bond make the CO vibrational frequency a poor indicator of the surface bond strength. For symmetric N_2, there is no prepolarization of the 1π orbital by the 5σ orbital and the downward shift of the vibrational frequency associated with chemisorption should provide a much more direct measure of the $2\pi^*$ back-donation which is the major contributor to the adsorption bond strength.

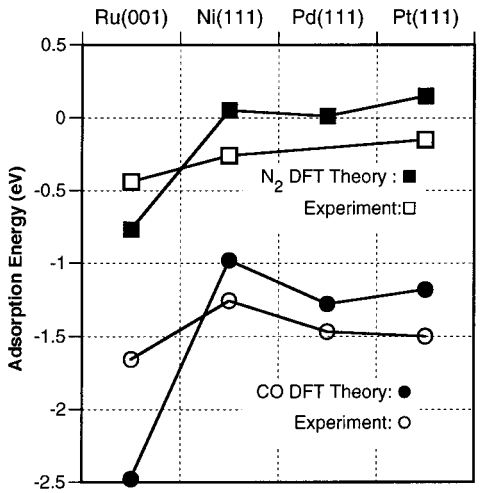

Figure 14. Predictions of Nørskov's parametric DFT model for CO (ref 45) and N_2 (ref 42) adsorption on some close-packed metal surfaces and a comparison to experimental values.[51,52]

Nørskov and co-workers have developed a simplified parametric model for CO (ref 45) and N_2 (ref 42) adsorption on transition metals based on their DFT calculations. The metal d band is considered as a single discrete state which interacts with the molecular 5σ and $2\pi^*$ states. The interaction energies with the metal sp states are approximated by full DFT calculations for N_2 and CO adsorbed on Al(111) (+0.3 and −0.4 eV, respectively).[42] Adding these energies to the values calculated for the d state interactions approximates the total adsorption energy. The predictions of this simple model for some close-packed metal surfaces for which experimental data exists are presented in Figure 14. Bond strengths to Ru are overestimated because the simple model parametrizes the d-band by only its mean energy, e_d, and does not account for the relatively broad d-bandwidth of Ru. Nevertheless, the trends of the experimental data seem adequately described by the simple theory. Although N_2 is predicted to be only on the verge of chemisorption for Ni(111) and Pd(111), it should be frankly unstable by 0.15 eV on Pt(111). Experimentally, both Ni(111)[29] and Pd (111)[46] support weakly chemisorbed N_2 at low temperatures. The XPS data reported here indicate that Pt(111) does not chemisorb N_2 except at substrate defects or as a minority species within islands of physisorbed N_2. The RAIRS data show that N_2 chemisorbs on the step defects of our Pt(111) surfaces. Nørskov's simple model predicts that N_2 chemisorbed at such defects (modeled as Pt(211) steps) should be 0.15 eV more stable than on the Pt(111) terrace. The enhanced stability results from an upward shift of the local d-band density of states at the top of the steps (moving e_d from −2.75 to −2.4 eV).[20] The predicted binding energy for chemisorbed N_2 at Pt(111) step defects is then the same as for the Ni(111) and Pd(111) terrace sites which experimentally chemisorb N_2. In this way, the simple electronic structure model for N_2 binding on transition metals provides a

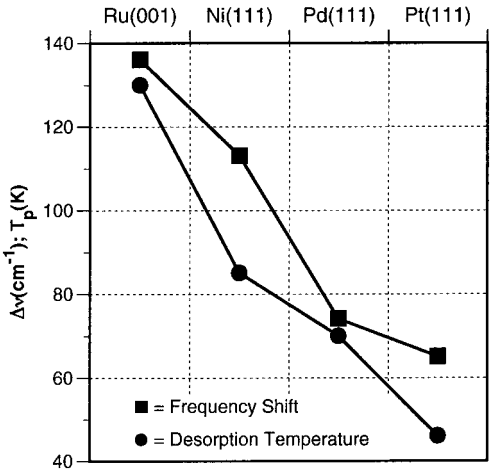

Figure 15. Desorption temperatures, T_p, and IR frequency shifts, $\Delta\nu = \nu(N_{2(g)}) - \nu(N_{2(ad)})$, for N_2 chemisorbed on some close-packed metal surfaces.[52]

rationale for the major features of N_2 binding on Pt(111): predominantly physisorption on the terraces and chemisorption at the defects. The calculations also place the energetics of N_2 adsorption on the Pt(111) terraces at the threshold between very weak chemisorption and physisorption.

It was suggested above that the frequency shift when N_2 chemisorbs on a transition metal might be a reasonable measure of the $2\pi^*$ back-donation which is the primary contributor to the adsorption energy. Figure 15 plots the desorption temperatures, T_p, and the frequency shifts, $\Delta\nu = \nu(N_{2(g)}) - \nu(N_{2(ad)})$, for N_2 chemisorbed on several close-packed metal surfaces. The molecules are presumed to be always chemisorbed vertically on top sites, as they are for Ru(001).[26] The entry for Pt(111) is based on the 2266 cm^{-1} RAIRS band observed for the minority of N_2 which was chemisorbed within the interior of physisorbed islands. According to RAIRS (Figure 4), these chemisorbed molecules desorbed at 46 K along with the island phase. Figure 15 indicates there is good correlation between $\Delta\nu$ and T_p, and by extension between $\Delta\nu$ and E_{ad}. On the basis of this correlation, we assign the 2266 cm^{-1} band to N_2 chemisorbed on top sites of the Pt(111) terraces.

B. Phase Behavior. The TPD, RAIRS, and photochemical data all provide evidence for a change in the characteristics of the adsorbed N_2 layer at a coverage of $\theta \sim 0.07$ monolayer. In analogy to the behavior of rare gases on close-packed metal surfaces such as W(110)[11] and Ru(001),[12] we interpret the change of the N_2/Pt(111) TPD kinetics from first to zeroth order as evidence for entry into a two-phase coexistence regime involving a dilute 2-D gas phase and a condensed island phase. On Ru(001), rare gases enter their two-phase coexistence regime at about 10% of their saturation coverage or roughly 0.05 monolayer in Pt(111) monolayer units. The 0.15 eV desorption energy of the dilute phase of N_2 on Pt(111) matches that for Kr on Ru(001) and similar phase behavior for these weak adsorption systems is expected.

In summary, although the N_2 adlayer on Pt(111) may not achieve complete thermal equilibrium after dosing at $T_s \leq 30$ K and certainly does not appear to remain at thermal equilibrium during laser irradiation, we tentatively suggest the phase diagram of Figure 16 may be useful for further discussion of N_2 on Pt(111). Photochemical arguments elaborated upon below in section 4.2 argue for the island phase being composed of seven-membered pinwheels similar to those observed by He beam diffraction for N_2 physisorbed on Cu(110).[37] The photochemical data may be rationalized if the 2-D gas phase is composed of

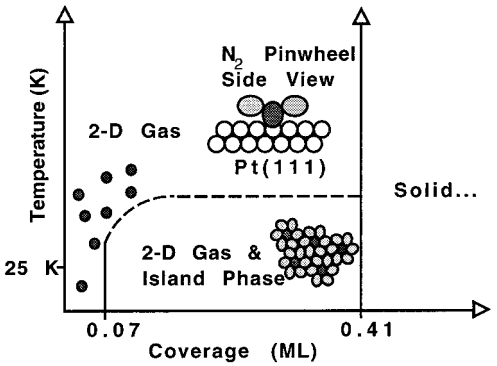

Figure 16. Proposed phase diagram for N_2 on Pt(111) at low temperature. The schematic structural cartoons depict vertically chemisorbed N_2 as dark gray and horizontally physisorbed N_2 as light gray.

vertically chemisorbed N_2 which can condense out to form the "pins" of the pinwheel island phase when decorated by "wheels" of horizontally oriented physisorbed molecules. The pinwheel phase of N_2 on Cu(110) is characterized by a saturation coverage of $\theta_{sat} = 0.46$ monolayer and a calculated adsorbate binding energy of $E_{ad} = 0.11$ eV, which compares to $\theta_{sat} = 0.41$ monolayer $\pm$ 10% and $E_{ad} = 0.13$ eV measured by TPD for the island phase on Pt(111). Quadrupolar interactions between physisorbed N_2 molecules are theoretically expected to produce pinwheel phases when the adsorbate/substrate interaction become sufficiently weak.[37] This energetic limit appears to have been reached for N_2/Pt(111) but with the caveat that the pin molecules are very weakly chemisorbed. Although our data are consistent with the phase diagram of Figure 16, independent verification of the pinwheel phase by a nondestructive structural probe such as He beam scattering or low-intensity LEED would be most helpful. In addition, although our XPS, TPD, and photochemical results argue for the photoinactive N_2 being physisorbed, and likely bound parallel to the surface, HREELS vibrational spectroscopy by impact and/or dipole scattering mechanisms could resolve these final structural issues about the N_2 island phase.

4.2. Photochemistry. The high translational energy of the laser-desorbed N_2 and the bimodal $P(E_T)$ indicate that the photodesorption is nonthermal in origin. A desorption mechanism involving direct localized absorption of light in a N_2/metal complex is discounted because the photodesorbing N_2 $P(E_T)$ did not vary as the photon energy was increased from 4.0 eV (308 nm) to 6.4 eV (193 nm) and more energy should have appeared as N_2 translation if direct photon absorption had occurred. Alternatively, the dynamics are consistent with the transfer of a photoexcited substrate electron to an affinity level of adsorbed N_2 lying beneath the vacuum level and desorption proceeding via Antoniewicz bounce dynamics. When the laser irradiates the surface, photoexcited electrons are produced in a continuum up to $E_F + h\nu$ and the nuclear dynamics following electron attachment to an adsorbate should be independent of photon energy as long as $E_F + h\nu$ remains above the top of the adsorbate affinity band.[3] The polarization dependence of the N_2 photodesorption yields (Figure 7) is certainly consistent with the electron transfer mechanism. Finally, we discount direct photochemistry in favor of photoinduced electron harpooning of N_2 because there is no gas phase photochemistry of N_2 at photon energies below 8.5 eV, whereas the $^2\Pi_g$ affinity level of $N_{2(g)}$ (EA = -2.3 eV) has been calculated to shift down *below* the vacuum level if the N_2 could be hypothetically adsorbed at chemisorptive distances of a few angstroms away from a Ag(111) surface.[5] Nørskov's parametrized DFT model for vertically chemisorbed N_2 on top sites of (111) transition

metals (Figure 14) presupposes a constant 1.94 Å adsorption height between the metal and inner nitrogen atomic cores. The correlations found in Figures 14 and 15 suggest that such an adsorption height of ~2 Å is reasonable for the minority of N_2 which is very weakly chemisorbed on Pt(111).

As discussed in section 3.5 above, the observation of wavelength-independent translational energy distributions for N_2 photodesorbing from 193 to 308 nm and the lack of photodesorption at 355 nm indicates that the entire affinity band lies between 3.5 and 4.0 eV above the Fermi level. A conservative lower bound for the work function of N_2/Pt(111) can be estimated as 5.25 eV given the $\phi = 5.8$ eV value for clean Pt(111) and the knowledge that a saturated layer of chemisorbed N_2 on Ru(001) reduces the work function by only 0.55 eV (i.e., $\Delta\phi = -0.55$ eV)[30] while $\Delta\phi \leq -0.1$ eV for physisorbed N_2 on Ag(111).[46] Estimating $\phi \geq 5.25$ eV for N_2/Pt(111), the affinity band of chemisorbed N_2 is located at least 1.25 eV below the vacuum level. The ~0.5 eV width of the affinity band is surprisingly narrow because the 0.53 eV wide $^2\Pi_g$ affinity band of gaseous N_2 is expected to broaden as the $2\pi^*$ orbital comes into overlap with the sp and d bands of the metal surface.[4,5,42]

HREELS has shown that the $^2\Pi_g$ affinity band of physisorbed N_2 on Ag(111) is located 1.2 eV *above* the vacuum level in good agreement with theory if the adsorption height is 3−4 Å above the surface.[5] The affinity band of bulk physisorbed N_2 is 0.8 eV above the vacuum level.[6] Coupled with the lower bound for the N_2/Pt(111) work function of 5.25 eV, the affinity levels of physisorbed N_2 within the monolayer and within a bulk multilayer on Pt(111) should be at least 6.45 and 6.05 eV above the Fermi level, respectively. Neither of these levels could be accessed by photoexcited substrate electrons stimulated by 4 eV photons at 308 nm where efficient N_2 photodesorption was observed. The lack of accessible low-lying electronically excited states of gas phase N_2 permits us to eliminate any form of physisorbed N_2 from participating in the 308 nm photodesorption of N_2 from Pt(111). Indeed, since the $P(E_T)$ of the photodesorbing N_2 remained invariant for photodesorption from 308 to 193 nm ($h\nu = 6.4$ eV), there does not appear to be any photoactivity attributable to physisorbed N_2 over this entire wavelength range. Certainly, there was no photodesorption at 193 nm from bulk multilayer deposits of physisorbed N_2 (Figure 11).

Only vertically chemisorbed N_2 on Pt(111) is expected to have an accessible affinity band at 3.5−4 eV above the Fermi level which could support the observed photodesorption at 308 nm. In consequence, we speculate that the two phases of N_2 on Pt(111) are an island phase of seven-membered N_2 pinwheels, in analogy to N_2 on Cu(110), and a 2-D gas of vertically chemisorbed N_2. The photochemical data of Figures 9, 10, and 11 suggest that the first ~0.07 monolayer of N_2 forms a 2-D gas of photoactive chemisorbed "pins" and subsequent N_2 physisorbs parallel to the surface in wheel structures which decorate the pins to form a pinwheel island phase. The local coverage of vertically chemisorbed molecules in the pinwheel islands will be one-seventh of the 0.41 monolayer saturation coverage, or 0.06 monolayer. These phases are decomposable into those required to support zeroth-order TPD[13] as discussed above: a 2-D gas of local coverage ~0.07 monolayer (over both substrate and islands) and a condensed island phase (represented here by the flat lying physisorbed N_2 within the pinwheels). Returning to Figure 9, the reduction in the photochemical cross section with coverage up until ~0.06 monolayer can be attributed to increased interadsorbate quenching as the

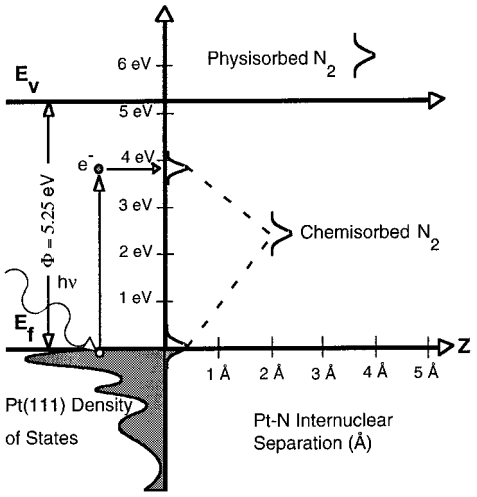

Figure 17. Proposed scheme for bonding and photoactivity of N_2 on Pt(111) with the work function set at an estimated lower bound of $\phi = 5.25$ eV.

distance between the photoactive, chemisorbed N_2 molecules is decreased. In Figure 11, the initial increase in the photodesorption yield with coverage, terminating in a plateau at ~0.07 monolayer, is again consistent with sequential chemisorption and physisorption of N_2. Although the chemisorbed 2-D gas/pinwheel island two-phase model can account for the photochemical and TPD results, the XPS and RAIRS data should be revisited. The XPS data showed no evidence for chemisorbed N_2 based on charge transfer screening of the N 1s core hole but this phenomenon should vanish in the limit of weak electronic coupling between the metal and adsorbate. We submit that the XPS results are consistent with the other theoretical (Figure 14) and experimental (Figure 15) data which indicate that N_2 is indeed very weakly chemisorbed on Pt(111). The remaining unusual observation is Figure 5 which shows that the low coverage 2-D gas of chemisorbed N_2 is RAIRS inactive but after a coverage of ~0.07 monolayer is exceeded the RAIRS band at 2266 cm^{-1} grows in approximately linearly with the pinwheel island coverage. We suspect that the very weak chemisorption of isolated N_2 molecules on the Pt(111) terraces does not introduce sufficient electronic asymmetry to induce a dipole derivative associated with the N_2 stretching mode which can be observed in our RAIRS spectra. However, when the local symmetry surrounding the chemisorbed N_2 "pins" is further reduced by a surrounding wheel of physisorbed molecules (see Figure 16) the dipole derivative along the surface normal may increase to RAIRS observable levels. In this manner, we may explain the appearance and increase of the 2266 cm^{-1} band as the pinwheel island phase grows in. Despite two potential stages of symmetry breaking, the RAIRS cross section for N_2 chemisorbed within the pinwheel islands is estimated to be an order of magnitude smaller than that for N_2 chemisorbed at defect sites (see Figure 5 and section 3.3).

Let us briefly return to discuss the bonding of chemisorbed N_2 on Pt(111) and the location of its photoactive affinity band with the aid of Figure 17. Far from the surface, the $^2\Pi_g$ affinity band of $N_{2(g)}$ with EA = −2.3 eV is a shape resonance associated with transiently trapping an electron into the empty $2\pi^*$ LUMO of $N_{2(g)}$. Experiment[7] and theory[5] indicate that this affinity band will drop to ~1.2 eV above the vacuum level when N_2 is physisorbed at 3−4 Å above a metal. At chemisorptive distances of ~2 Å, the N_2 molecular orbitals can begin to have significant overlap with the electron density of the metal surface. Nørskov's DFT analysis[42] of the Blyholder model[43] of N_2

bonding to transition metals begins with coupling the metal sp band to the molecular states and subsequently coupling the hybrid states to the metal d band. After the initial coupling of the $2\pi^*$ orbital to the Pt(111) sp band the "renormalized" $2\pi^*$ band of N_2, which is relevant to forming hybrid states with the metal d-band, is located 2.5 eV above the Fermi level in Nørskov's model. Bonding and antibonding (with respect to the surface) hybrid $2\pi^*$ affinity bands result from coupling of the N_2 renormalized $2\pi^*$ band with the metal d-band as illustrated schematically in Figure 17. The $2\pi^*$ bonding affinity band must be partially occupied for the experimentally observed chemisorption to occur and this is roughly predicted by Nørskov's parametrized DFT theory (Figure 14). Inverse photoemission spectroscopy (IPES) places the $2\pi^*$ antibonding affinity band at 1.6, 4.1, and 4.3 eV above the Fermi level for NO, CO, and N_2, respectively, on Ni(100),[47] whereas this band lies at 4.8 eV for CO on Pt(111).[48] Our photochemical data indicate there is an affinity band of chemisorbed N_2 on Pt(111) at 3.5−4 eV above the Fermi level and we surmise that this is the $2\pi^*$ antibonding affinity band as illustrated in Figure 17. Norskov's parametrized DFT model of CO and N_2 binding on transition metals[42] places the renormalized $2\pi^*$ band for both CO and N_2 at 2.5 eV above the Fermi level and given that the $2\pi^*$/d-band overlap integrals are less for N_2 than CO it seems reasonable that the N_2 $2\pi^*$ antibonding affinity band should lie lower in energy than the 4.8 eV band for CO. It is worth repeating that the apparent 0.5 eV width of the N_2/Pt(111) $2\pi^*$ antibonding affinity band as delineated by the photodesorption action spectrum is remarkably narrow.

A schematic of the proposed mechanism for photodesorption is given in Figure 17. Light absorption creates photoexcited hot substrate electrons which can access the $2\pi^*$ antibonding affinity band of N_2 on Pt(111). The ensuing dynamics on the charge transfer excited state will be quenched on a 1−100 fs time scale. If the excited state potential is attractive as one might expect based on image attraction for the anion, Antoniewicz bounce dynamics should lead to desorption.[8] If the excited state is repulsive, then Menzel−Gomer−Redhead[49] (MGR) dynamics should apply. In the MGR mechanism, if sufficient energy in the repulsive excited state can be accumulated before quenching onto the ground state potential, then desorption will occur directly without an intervening collision with the surface as in the Antoniewicz bounce mechanism. Theoretical and experimental studies of NO/Pt(111) photodesorption,[50] which appears to be a system quite analogous to N_2/Pt(111), suggest that the dynamics are of the Antoniewicz type. Unfortunately, the experiments reported here cannot resolve between these two detailed desorption dynamics. For either dynamics, decreasing the femtosecond time scale for quenching the adsorbate excited state leads to less efficient desorption. The lack of photodesorption from chemisorbed N_2 on the Pt(111) step edges (defects) may be due to enhanced quenching of the N_2 excited states at the defects as compared to quenching on the Pt(111) terraces, or due to the higher ground state binding energy for N_2 at the defects (particularly, if MGR dynamics apply).

5. Conclusions

To summarize, the N_2 adlayer ($\theta_{sat} = 0.41$ monolayer $\pm$ 10%) on Pt(111) contains a minority of photoactive, weakly chemisorbed N_2 ($\theta_{chemi} \sim 0.07$ monolayer) assigned as vertically bound at Pt(111) top sites by RAIRS, and a majority of photoinactive molecules assigned as physisorbed by XPS. Thermal programmed desorption, reflection−absorption infrared spectroscopy (RAIRS), and photodesorption data gave evidence for two-phase coexistence between a 2-D gas phase of chemisorbed N_2 and a condensed N_2 island phase at coverages $\theta \geq 0.07$ monolayer. The data are broadly consistent with the speculation that the condensed island phase is composed of seven-membered "pinwheels" in which vertically chemisorbed N_2 "pins" are decorated by "wheels" of horizontally oriented physisorbed molecules. Only the weakly chemisorbed N_2 on terrace sites exhibited photodesorption under laser irradiation in the ultraviolet. The N_2 photodesorption experiments are consistent with a desorption mechanism involving transient attachment of a photoexcited substrate electron into an affinity band of chemisorbed N_2 which lies between 3.5 and 4.0 eV above the Fermi level. The photoactive affinity band is presumed to be the $2\pi^*$ antibonding band which has been observed in IPES on other metals.

The photochemical experiments were particularly useful for confirming the RAIRS assignment that a fraction of the N_2 adlayer was chemisorbed on Pt(111), even though XPS showed no spectral signature of chemisorbed N_2 as known from other metals. It is interesting to note that the internal electronic structure of an adsorbate, such as N_2 on Pt(111) top sites or CO on Pt(111) 3-fold hollow sites,[9] may become considerably rearranged by chemisorption yet still display a net adsorption energy of only a few tenths of an electronvolt. We speculate that such weakly bound species whose internal bonds are substantially weakened and which can be conveniently studied at low temperature may have some catalytic relevance to reactions performed at much higher temperatures and pressures. Finally, although there was no evidence for photoinduced dissociation of N_2 on Pt(111), it is worth noting that the ability to use light to electron harpoon and accelerate a species such as N_2 toward a catalytic metal surface with mean translational energies equivalent to temperatures of ~1450 K might find use in catalysis if the process were to result in significant dissociative adsorption.

Acknowledgment. Financial support by the National Science Foundation, Grant CHE-9634272 is gratefully acknowledged.

Note Added in Proof. A very recent paper[53] on higher temperature N_2 adsorption on stepped Pt(111) surfaces employing RAIRS and DFT theoretical analysis confirms that the 2234 cm^{-1} N_2 band derives from N_2 vertically chemisorbed on step edge sites.

References and Notes

(1) Somorjai, G. A. *Introduction to Surface Chemistry and Catalysis*; John Wiley & Sons: New York, 1994.

(2) Davies, J. A.; Boucher, D. L.; Edwards, J. G. *Adv. Photochem.* **1995**, *19*, 235.

(3) Harrison, I. In *Laser Spectroscopy and Photochemistry on Metal Surfaces*; Dai, H.-L., Ho, W., Eds.; Advanced Series in Physical Chemistry, Vol. 5; World Scientific Press: Singapore, 1995; Chapter 27.

(4) Harris, S. M.; Holloway, S. *Chem. Phys. Lett.* **1995**, *243*, 393.

(5) Rous, P. J. *Phys. Rev. Lett.* **1995**, *74*, 1835.

(6) Bader, G.; Perluzzo, G.; Caron, L. G.; Sanche, L. *Phys. Rev. B* **1984**, *30*, 78.

(7) Demuth, J. E.; Schmeisser, D.; Avouris, Ph. *Phys. Rev. Lett.* **1981**, *47*, 1166.

(8) Antoniewicz, P. R. *Phys. Rev. B* **1980**, *21*, 3811.

(9) Nekrylova, J.; French, C.; Artsyukhovich, A.; Ukraintsev, V.; Harrison, I. *Surf. Sci.* **1993**, *295*, L987.

(10) Schlichting, H.; Menzel, D. *Rev. Sci. Instrum.* **1993**, *64*, 2013.

(11) Opila, R.; Gomer, R. *Surf. Sci.* **1981**, *112*, 1.

(12) Schlichting, H.; Menzel, D. *Surf. Sci.* **1992**, *272*, 27.

(13) Kreuzer, H. J.; Payne, S. H. *Surf. Sci.* **1988**, *198*, 235. Payne, S. H.; Kreuzer, H. J. *Surf. Sci.* **1988**, *205*, 153.

(14) Bolz, L. H.; Boyd, M. E.; Mauer, F. A.; Perser, H. S. *Acta Crystallogr.* **1959**, *12*, 249.

(15) Breitschafter, M. J.; Umbach, E.; Menzel, D. *Surf. Sci*. **1986**, *178*, 725.
(16) Artsyukhovich, A. N.; Ukraintsev, V. A.; Harrison, I. *Surf. Sci*. **1996**, *347*, 303.
(17) Head-Gordon, M.; Tully, J. C.; Schlichting, H.; Menzel, D. *J. Chem. Phys.* **1991**, *95*, 9266.
(18) Shigeishi, R. A.; King, D. A. *Surf. Sci.* **1977**, *62*, 379.
(19) Arumainayagam, C.; Tripa, C.; Xu, J.; Yates, J. *Surf. Sci*. **1996**, *360*, 121.
(20) Hammer, B.; Nielsen, O. H.; Nørskov, J. K. *Catal. Lett.* **1997**, *46*, 31.
(21) Campbell, J. H.; Bater, C.; Durrer, W. G.; Craig, J. H. *Surf. Sci.* **1997**, *380*, 17.
(22) Tillborg, H.; Nilsson, A.; Hernnäs, B.; Mårtensson, N.; Palmer, R. E. *Surf. Sci*. **1993**, *295*, 1.
(23) Björneholm, O.; Nilsson, A.; Sandell, A.; Hernnäs, B.; Mårtensson, N. *Phys. Rev. Lett*. **1992**, *68*, 1892.
(24) Umbach, E. *Solid State Commun*. **1984**, *51*, 365.
(25) Nilsson, A.; Tillborg, H.; Mårtensson, N. *Phys. Rev. Lett.* **1991**, *67*, 1015.
(26) Bludau, H.; Gierer, M.; Over, H.; Ertl, G. *Chem. Phys. Lett*. **1994**, *219*, 452.
(27) Grunze, M.; Golze, M.; Hirschwald, W.; Freund, H. J.; Pulm, H.; Seip, U.; Tsai, M. C.; Ertl, G.; Küppers, J. *Phys. Rev. Lett.* **1984**, *53*, 850.
(28) Brubaker, M. E.; Trenary, M. *J. Chem. Phys*. **1986**, *85*, 6100.
(29) Yoshinobu, J.; Zenobi, R.; Xu, J.; Xu, Z.; Yates, J. T. *J. Chem. Phys.* **1991**, *95*, 9393.
(30) de Paola, R. A.; Hoffmann, F. M.; Heskett, D.; Plummer, E. W. *Phys. Rev. B* **1987**, *35*, 4236.
(31) Gardner, P.; Martin, R.; Tushaus, M.; Shamir, J.; Bradshaw, A. M. *Surf. Sci.* **1993**, *287/288*, 135.
(32) Micheley, T.; Land, T.; Littmark, U.; Comsa, G. *Surf. Sci.* **1992**, *272*, 204.
(33) Reutt-Robey, J. E.; Doren, D. J.; Chabal, Y. J.; Christman, S. B. *J. Chem. Phys*. **1990**, *93*, 9113.
(34) Herzberg, G. *Spectra of Diatomic Molecules*; Van Nostrand Reinhold Co.: New York, 1950; p 62.
(35) Persson, B. N. J.; Ryberg, R. *Phys. Rev. B* **1981**, *24*, 6954.
(36) Xu, Z.; Sherman, M. G.; Yates, J. T.; Antoniewicz, P. R. *Surf. Sci*. **1992**, *276*, 249.
(37) Zeppenfeld, P.; George, J.; Diercks, V.; Halmer, R.; David, R.; Comsa, G.; Marmier, A.; Ramseyer, C.; Girardet, C. *Phys. Rev. Lett*. **1997**, *78*, 1504.
(38) Amorelli, T. S.; Carley, A. F.; Rajumon, M. K.; Roberts, M. W.; Wells, P. B. *Surf. Sci*. **1994**, *315*, L990.
(39) Richter, L. J.; Buntin, S. A.; King, D. S.; Cavanagh, R. R. *Chem. Phys. Lett.* **1991**, *186*, 423.
(40) Weik, F.; de Meijere, A.; Hasselbrink, E. *J. Chem. Phys.* **1993**, *99*, 682.
(41) Lin, J. C.; Gomer, R. *Surf. Sci*. **1989**, *218*, 406.
(42) Mortenson, J. J.; Morikawa, Y.; Hammer, B.; Nørskov, J. K. *Z. Phys. Chem.* **1997**, *198*, 113.
(43) Blyholder, G. *J. Phys. Chem.* **1964**, *68*, 2772.
(44) Bagus, P. S.; Pacchioni, G. *Surf. Sci*. **1992**, *278*, 427.
(45) Hammer, B.; Morikawa, Y.; Nørskov, J. K. *Phys. Rev. Lett.* **1996**, *76*, 2141.
(46) Bertolo, M.; Jacobi, K. *Surf. Sci.* **1992**, *265*, 1.
(47) Johnson, P. D.; Hulbert, S. L. *Phys. Rev. B* **1987**, *35*, 9427.
(48) Dose, V. *Surf. Sci. Rep.* **1986**, *5*, 337.
(49) Menzel, D.; Gomer, R. *J. Chem. Phys.* **1964**, *40*, 1164; **1964**, *41*, 3311. Redhead, P. A. *Can. J. Phys.* **1964**, *42*, 886.
(50) Zimmerman. F. W.; Ho, W. *Surf. Sci. Rep.* **1995**, *22*, 127, and references therein.
(51) CO experimental values from ref 45.
(52) N_2 experimental values from ref 30 for Ru(001), ref 29 for Ni-(111), ref 46 for Pd(111), and this work for Pt(111).
(53) Tripa, C. E.; Zubkov, T. S.; Yates, J. T., Jr.; Mavrikakis, M.; Nørskov, J. K. *J. Chem. Phys.* **1999**, *111*, 8651.